






# Photoacoustic imaging of microenvironmental changes in facial cupping therapy

YINGYING ZHOU,<sup>1,2,3,6</sup>  FEI CAO,<sup>1,3,6</sup> HUANHAO LI,<sup>1,3</sup>  XIAZI HUANG,<sup>1,3</sup> DONGSHAN WEI,<sup>5</sup>  LIDAI WANG,<sup>2,4,7</sup> AND PUXIANG LAI<sup>1,3,8</sup> 

<sup>1</sup>Department of Biomedical Engineering, The Hong Kong Polytechnic University, Hong Kong

<sup>2</sup>Department of Biomedical Engineering, City University of Hong Kong, Hong Kong

<sup>3</sup>The Hong Kong Polytechnic University Shenzhen Research Institute, Shenzhen, China

<sup>4</sup>City University of Hong Kong Shenzhen Research Institute, Shenzhen, China

<sup>5</sup>School of Electrical Engineering and Intelligentization, Dongguan University of Technology, Dongguan, China

<sup>6</sup>These authors contributed equally to this work

<sup>7</sup>lidawang@cityu.edu.hk

<sup>8</sup>puxiang.lai@polyu.edu.hk

**Abstract:** As a traditional medicine practice, cupping therapy has been widely used to relieve symptoms like fatigue, tension, and muscle pain. During the therapy, negative pressure is applied to the skin for a while with an intention to enhance blood circulation or induce micro-bleeding. The therapeutic effect, however, is not clear due to the lack of direct quantification. Aiming at a quantitative assessment of the treatment effect, we explore optical-resolution photoacoustic microscopy (OR-PAM) in monitoring the structural and functional changes after cupping. We find that, after 5-minutes of ~ 20 kPa negative pressure cupping, more capillaries appear in the focus, and micro-bleeding is observed from the capillaries. We quantify the images and find the blood vessel density is increased by 64%, and the total hemoglobin concentration in both the veins and the arteries exhibits 62% and 40% elevation, respectively. Oxygen saturation in the vein and artery decreased by 17% and 3% right after cupping, respectively. After two hours of recovery, the three blood-related parameters return to their original levels, indicating that the effects in the tissue last only a short period after cupping at the given pressure and time duration. Note that no significant cupping marks are induced with the treatment parameters in this study. This work proposes OR-PAM to quantitatively monitor and evaluate the effect of cupping therapy from the perspective of imaging. The method is also useful for accurate control of the therapeutic outcome.

© 2020 Optical Society of America under the terms of the [OSA Open Access Publishing Agreement](#)

## 1. Introduction

Cupping therapy is a traditional medicine practice that applies negative pressure to the skin, leading to increased blood circulation or micro-bleeding in local tissue. It is claimed that cupping can increase capillary permeability, enhance tissue gas exchange, promote blood circulation, and relieve symptoms like fatigue, tension, and muscle pain [1,2]. After cupping treatment, marks caused by capillary expansion or micro-bleeding may appear on the skin surface. They usually exhibit skin protrusions of different colors, yet sometimes bleeding points and blisters may show up due to excessive negative pressure and long treatment time [3].

Cupping therapy has been used for thousands of years to relieve soreness and pain [4]. Nowadays, the clinical practices of cupping have extended, such as to treat herpes zoster, acne vulgaris, cervical spondylosis, cough, scapula, peri-arthritis of the shoulder and facial paralysis [5–15]. However, due to the lack of quantitative assessment tools, the effectiveness, the optimal negative pressure and time duration of cupping therapy have not been thoroughly

studied. Recently, some researchers have interpreted cupping therapy from the perspective of microenvironment changes based on parameters obtained from optical sensing tools. For example, in 2017, Li *et al.* used near-infrared spectroscopy to investigate the hemodynamics in the tissue around the cupping site [16]. A significant drop in deoxyhemoglobin but an elevation in oxyhemoglobin was recorded, indicating an enhancement of oxygen uptake around the cupping site. Right at the cupping site, in 2019 the same team reported increased deoxyhemoglobin but declined oxyhemoglobin [17]. The results from these two studies are quite consistent, suggesting improved blood circulation due to the cupping treatment. Similar measurements were repeated by Jae Gwan *et al.*, who embedded an optical sensor within the therapy cup to monitor the hemodynamic changes during cupping [18]. They observed elevation of both deoxyhemoglobin and oxyhemoglobin at the cupping site but drop of both parameters at the surrounding positions, confirming cupping can increase the oxygen and blood supplement to cupping site.

Although promising, the aforementioned studies are based on optical sensing, which results in spatially averaged measurements. It is preferred if the microenvironment parameter changes can be spatially resolved and mapped to the micro-circulation system. Therefore, high-resolution optical imaging is desired for cupping assessment. Taking advantage of optical absorption contrast and subcellular spatial resolution, optical-resolution photoacoustic microscopy (OR-PAM) is exploited in this study to image the microenvironmental changes [19–25] in cupping. OR-PAM can provide label-free quantitative imaging of the micro-vessels and oxygen saturation *in vivo* [26,27]. Cupping with low negative pressure and photoacoustic (PA) imaging is performed on the mouse ear. The dynamic change in the treated tissue is recorded using OR-PAM. Structural and functional parameters, including the total hemoglobin concentration, vascular density, and oxygen saturation, are quantitatively monitored from the images in the whole process of cupping.

## 2. Methods

A schematic of OR-PAM is shown in Fig. 1. A 532-nm pulsed laser (7 ns pulse width, VPFL-G-20, Spectra-Physics) provides the excitation laser source. The 532-nm laser beam is divided into two paths by a polarizing beamsplitter (PBS1, PBS051, Thorlabs Inc). A half-wave plate (HWP1, GCL-060633, Daheng Optics) is placed before the PBS to adjust the energy ratio between the two daughter paths. One path transmits in free space, with a half-wave plate (HWP3) and a polarization beamsplitter (PBS2) to produce a small portion of the light to be sampled by a photodiode to monitor and compensate for the laser fluctuations. The other path is coupled into a 100-m multimode fiber (MMF, GIMMSC (50/125) P, Fibercore) to generate a 558-nm wavelength via the Stimulated Raman Scattering (SRS) effect [28,29]. To maximize the SRS efficiency, another half-wave plate (HWP2) is put before the 100-m fiber to tune the polarization state of the input beam. In addition, the 100-m MMF causes ~ 500-ns delay with respect to the other path. In order to pass the 558-nm wavelength and reject others, a band-pass filter (central wavelength 558 nm, bandwidth 10 nm, FB560-10, Thorlabs Inc) is placed after the MMF fiber. The two laser beams are recombined by a dichroic mirror (T550lpxr-UF1, CHROMA). The combined beams are coupled into a 2-m single-mode fiber (SM, P1-460B-FC-2, Thorlabs Inc) and delivered to the OR-PAM probe. The two sequential laser pulses at 532 nm and 558 nm are focused on the sample through the probe, generating two temporally separated PA signals. The energy applied to the mouse ear is about 50 nJ per pulse. An optical/acoustic beam combiner in the PA probe reflects the optical beam and transmits the ultrasonic beam. A 50-MHz piezoelectric transducer (V214-BC-RM, Olympus-NDT) detects the ultrasonic waves. We align the optical excitation beam with the acoustic detection beam coaxially and confocally to optimize the sensitivity. Raster scanning the PA probe allows for acquiring volumetric images. It takes ~ 16 minutes to acquire a PA image of  $2.5 \times 2.5 \text{ mm}^2$ . The imaging resolution is  $5 \mu\text{m}$  in the transverse plane and  $40 \mu\text{m}$  along the acoustic axial direction.

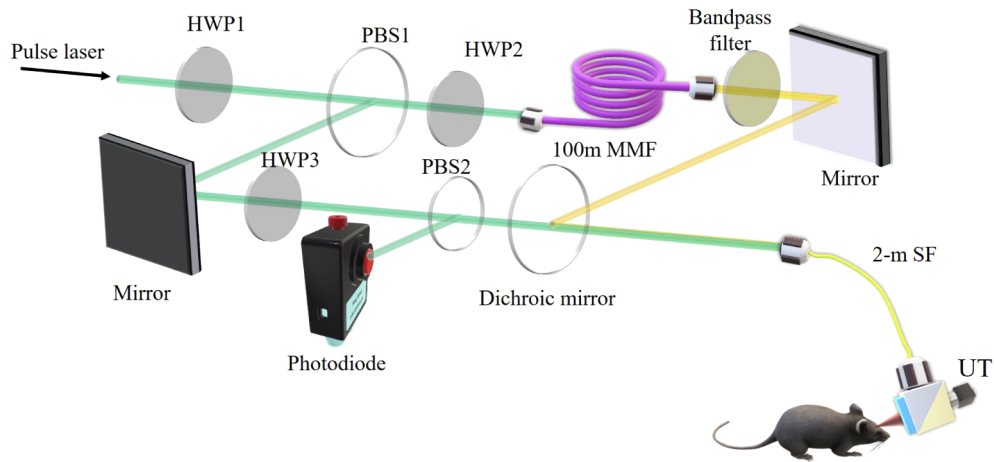


**Fig. 1.** Schematic of the photoacoustic-based microenvironment monitoring system. HWP1-3, half-wave plate; MMF, multimode fiber; PBS1-2, polarizing beamsplitter; SF, single-mode fiber; UT, ultrasound transducer.

In experiment, a 6-week ICR mouse was anesthetized with isoflurane, and the mouse ear was mounted on a glass platform with double-sided tape. All procedures involving animal experiments were approved by the animal ethical committee of the City University of Hong Kong. Before cupping therapy, we first acquired a PA image as a baseline. Then, a facial cup was applied to the mouse ear for 5 minutes. The outer and inner diameters of the facial cup opening are 1.5 cm and 0.7 cm, respectively, and the cup length is 5 cm. As a result, the region of the cupping area is around  $1.54 \text{ cm}^2$  in the experiment. The pressure exerted on the mouse ear was about -20 kPa. After the cupping process, we acquired several PA images with a time interval of two hours (including the pre-processing time and the imaging time; the actual resting time for the mouse is about 1 hour, which is comparable with the operation time) to monitor the microenvironment changes at the region of interest. Based on these images, blood vessel density, total hemoglobin concentration, and oxygen saturation are computed and analyzed.

### 3. Results and discussion

Structural images of the same region on the mouse ear pre- and post-cupping are shown in Fig. 2(a) and (b). Compared with the pre-cupping image, 64% more blood vessels (corresponding to vascular density, the calculation method mentioned in the following part) show up in the image right after the cupping. Moreover, the blood vessels' PA signal (the averaged PA intensity of the whole figure) increases  $\sim 37\%$  after cupping. Figure 2(c) and (d) are the close-up of white dashed boxes in (a) and (b), respectively. Thus, blood in vessels contributes to the majority of the PA signals in this scenario, and more small blood vessels lead to stronger PA intensities after the cupping. Thus, due to the cupping, more capillaries are congested under the negative pressure and more blood flow into the optical focus, the field of view of the PA imaging system. PA intensities from other small and large blood vessels pre- and post-cupping have not expressed many differences, indicating that this phenomenon is caused by the cupping effect rather than the optical focus changes. Benefiting from the high resolution, we can even clearly see micro-bleeding in the tissue, as pointed by the arrows. It takes about 16 minutes to acquire an image. Although slow, such an imaging speed has not influenced the results due to the fast B-scan speed, and the obtained figures have a relatively constant background (large blood vessels in a and b show close PA intensities).

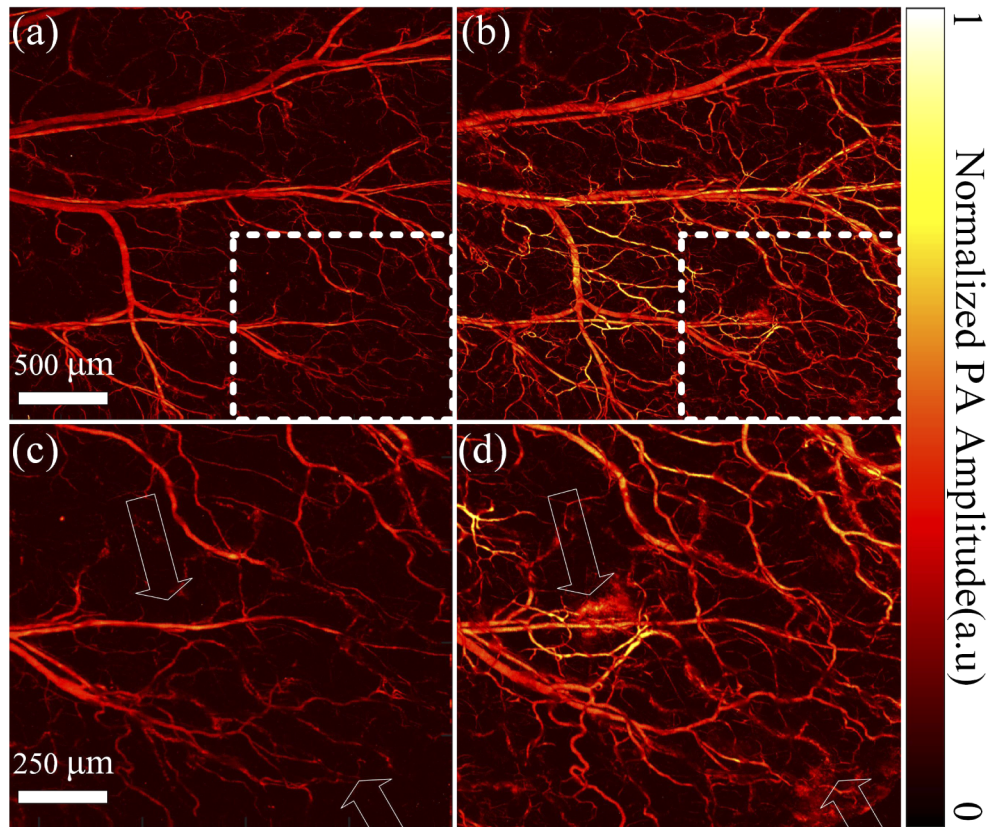


**Fig. 2.** OR-PAM structural imaging of the same region of a mouse ear before (a) and right after (b) cupping. (c) Close-up of the dashed box in (a). (d) Close-up of the dashed box in (b).

As a qualitative verification, we acquired a series of photographs before and after cupping, as shown in Fig. 3(a). The camera settings remained unchanged during the whole process. In the photographs, the mouse ear surface as a whole turned red right after the cupping and then recovered to the original status two hours later. Due to the low contrast, photographs cannot provide more detailed information. In contrast, as shown in Fig. 3(b), OR-PAM images of the same mouse ear as circled in Fig. 3(a) were acquired at 532 nm. PA signal strength (the averaged PA intensity of the whole figure) significantly increases  $\sim 37\%$  right after the cupping but recovers to its original level in two hours. After two hours, there are no significant changes in the PA signal strength. No cupping marks were left after the treatment. Two pairs of blood vessels in Fig. 3(b) are chosen to analyze the changes of normalized hemoglobin concentration in cupping through PA signal intensity at 532 nm. Because the absorption coefficients of deoxyhemoglobin and oxyhemoglobin are almost the same at 532 nm, the PA intensity is calibrated to measure the total hemoglobin concentration [30]. As shown in Fig. 3(c), both the veins and arteries exhibit increased hemoglobin concentration significantly right after the cupping. The hemoglobin concentration increased 62% in the veins and 40% in the arteries (forty  $10 \times 10$ -pixel areas in the blood vessel are calculated,  $p < 0.05$  from One-way ANOVA, and the sample size is 40). The observed increase is highly consistent with the photographic and morphological PA imaging results in Fig. 3(a) and (b). After two hours, the hemoglobin concentration in the arteries and veins declines to their original levels. Based on the PA images in Fig. 3(b), we quantify the blood



vessel density. Four times of the standard deviation of the background is used as a threshold to extract the vascular signals. The number of pixels occupied by blood vessels is counted, from which the vascular density is estimated as the ratio between the vessel pixel number and the total pixel number. The vascular density increases by 64% right after the cupping. After the negative pressure is removed, the vessels and capillaries recover back to their original states, and so does the vascular density. Collectively, the changes in the ear photographs and PAM images, and the calculated total hemoglobin concentration and vascular density consistently suggest that the facial cupping treatment does boost the local blood perfusion. With 5 minutes of  $\sim 20$  kPa pressure, the local microenvironment recovers within two hours.

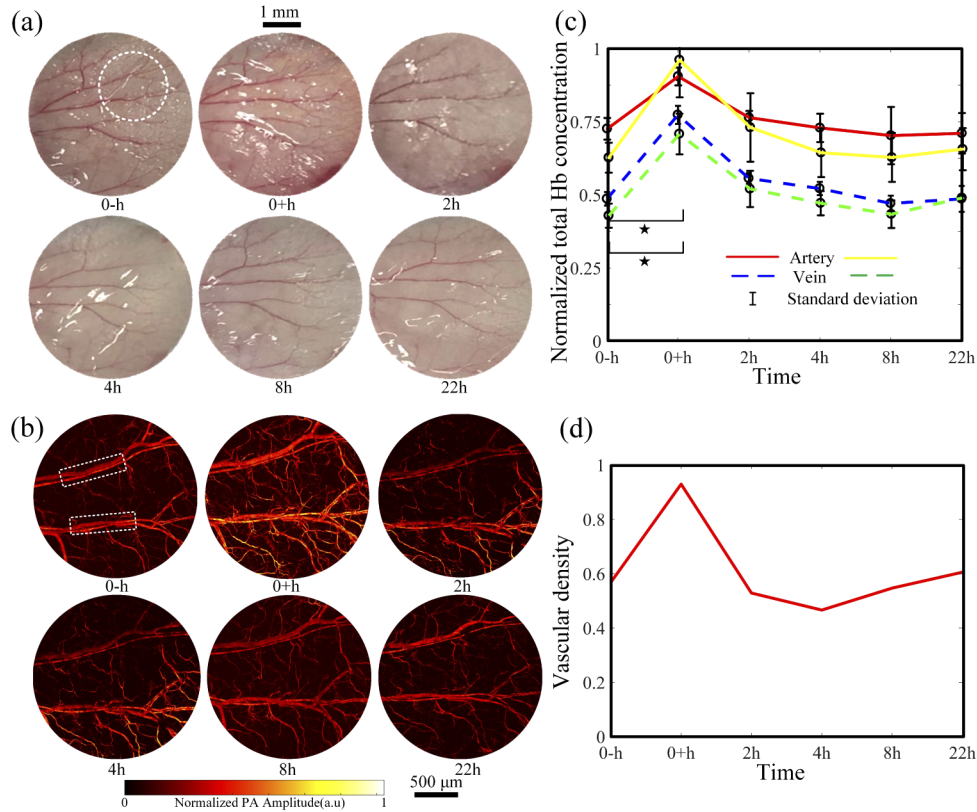


**Fig. 3.** Ear vessel photographs (a), OR-PAM images (b), total hemoglobin concentration (c), and vascular density (d) changes before and after the cupping treatment. In (c), changes of artery and vein within the white box in (b) are presented with the red (yellow) line and blue (green) dashed line, respectively.  $\star$ ,  $p < 0.05$  (tested by one way ANOVA). The error bars in (c) are standard deviations.

We further quantify the oxygen saturation ( $sO_2$ ) in the microenvironment through [31]

$$sO_2 = \frac{\varepsilon_{de}(\lambda_{558})P(\lambda_{532}) - \varepsilon_{de}(\lambda_{532})P(\lambda_{558})}{[\varepsilon_{ox}(\lambda_{532}) - \varepsilon_{de}(\lambda_{532})]P(\lambda_{558}) - [\varepsilon_{ox}(\lambda_{558}) - \varepsilon_{de}(\lambda_{558})]P(\lambda_{532})} \quad (1)$$

where  $\varepsilon_{ox}$  and  $\varepsilon_{de}$  are the molar extinction coefficients of oxy- and deoxyhemoglobin at 532 or 558 nm, PA is the photoacoustic signal amplitude at the two wavelengths. In Fig. 4(a), the  $sO_2$  images at different time points are computed. The  $sO_2$  value in the artery is higher than that in the vein. As shown in Fig. 4(b), the average  $sO_2$  values change with time in the regions labeled with the white box. The  $sO_2$  values in the veins are from 0.5 to 0.7, and above 0.95

in the arteries. Right after the cupping, the  $sO_2$  values in veins and arteries reduced by 17% and 3% (forty 10x10-pixel areas in the blood vessel were chosen for calculation;  $p < 0.05$  from One-way ANOVA, and the sample size is 40), respectively. The decrease of  $sO_2$  values in blood vessels indicates that more oxygen is consumed in the cupping site or has been transported to the surrounding tissues, promoting the metabolism at the cupping site. During the recovering process, the  $sO_2$  values in both veins and arteries return to their original levels. The results are consistent with Fig. 3 and other reports [16–18].

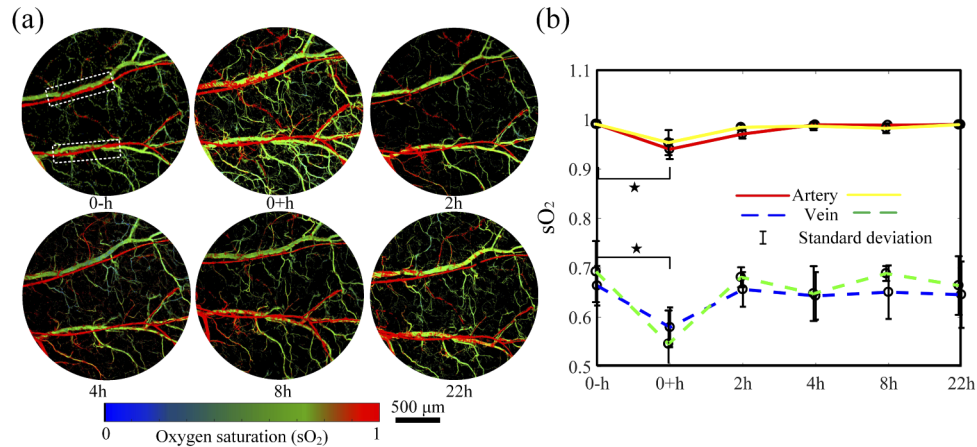


**Fig. 4.** Dynamic changes in oxygen saturation before and after cupping. (a)  $sO_2$  map of the mouse ear within the cupping process. (b) Averaged  $sO_2$  changes of the artery (red/yellow line) and the vein (blue/green dashed line) for regions labeled with the rectangle in (a). \*,  $p < 0.05$  (tested by One-way ANOVA). The error bars in (b) are standard deviations.

#### 4. Conclusion

To better understand the mechanism and quantify the effectiveness of cupping therapy, we introduce OR-PAM to investigate microenvironment changes before and after cupping practice. Considering the imaging depth of OR-PAM is limited within 1 mm, living mouse ear is chosen as the cupping site in this study for its appropriate thickness of around several hundred micrometers (100  $\mu\text{m}$ ). Although not perfect, such a model, as shown in this study, is sufficient to support OR-PAM to monitor and quantify the microenvironment changes associated with cupping therapy. As seen, right after the cupping, superficial capillaries have 37% stronger PA intensity compared with the pre-treatment ones. Some capillaries may bleed under the negative pressure. The total hemoglobin concentration in both veins and arteries is elevated significantly right after the cupping treatment, suggesting that cupping enhances blood circulation. In addition, more oxygen is consumed at the cupping site or stimulated to be transported to capillaries and the adjacent tissues out of the field of view, promoting the metabolism at the cupping site. In two hours after the cupping, the parameters go back to their original level in pre-cupping. This result shows that facial cupping ( $\sim 20$  kPa in 5 minutes) produces a temporary effect and does not cause long-time marks in the skin. In cupping with higher pressure and longer time, marks may stay up to weeks, indicating a more sustainable treatment effect, which, however, waits for further confirmation. The results are well consistent with other reported findings [16,17]. This pilot study is the first step to interpret cupping from a microscopic imaging perspective. We show that the use of OR-PAM can monitor and quantify the cupping effect with high spatial resolution, which can be further used to optimize the pressure and time duration of the cupping treatment. Future

explorations will move onto human patients, and acoustic resolution photoacoustic imaging will be used to visualize deeper (mm~cm) microenvironmental changes due to cupping.

## Funding

National Natural Science Foundation of China (81627805, 81671726, 81930048); Hong Kong Innovation and Technology Commission (ITS/022/18); Research Grants Council, University Grants Committee (11101618, 11215817, 21205016, 25204416); Shenzhen Science and Technology Innovation Commission (JCYJ20160329150236426, JCYJ20170413140519030, JCYJ20170818104421564).

## Disclosures

L.W. has a financial interest in PATech Limited, which, however, did not support this work.

## References

1. J. I. Kim, M. S. Lee, D. H. Lee, K. Boddy, and E. Ernst, "Cupping for treating pain: A systematic review," *Evid. Based Complement. Alternat. Med.* **2011**, 1–7 (2011).
2. H. J. Cao, M. Han, X. Li, S. J. Dong, Y. M. Shang, Q. A. Wang, S. Xu, and J. P. Liu, "Clinical research evidence of cupping therapy in China: a systematic literature review," *BMC Complementary Altern. Med.* **10**(1), 70 (2010).
3. P. Mehta and V. Dhapte, "Cupping therapy: A prudent remedy for a plethora of medical ailments," *J. Tradit. Complement. Med.* **5**(3), 127–134 (2015).
4. N. A. Qureshi, G. I. Ali, T. S. Abushanab, A. T. El-Olemy, M. S. Alqaed, I. S. El-Subai, and A. M. N. Al-Bedah, "History of cupping (hijama): a narrative review of literature," *J. Integr. Med.* **15**(3), 172–181 (2017).
5. H. J. Cao, C. J. Zhu, and J. P. Liu, "Wet cupping therapy for treatment of herpes zoster: A systematic review of randomized controlled trials," *Altern. Ther. Health Med.* **16**, 48–54 (2010).
6. H. J. Cao, J. P. Liu, and G. T. Lewith, "Traditional Chinese medicine for treatment of fibromyalgia: A systematic review of randomized controlled trials," *J. Altern. Complement. Med.* **16**(4), 397–409 (2010).
7. H. J. Cao, H. Hu, B. Colagiuri, and J. P. Liu, "Medicinal cupping therapy in 30 patients with fibromyalgia: A case series observation," *Forsch Komplementmed.* **18**(3), 3 (2011).
8. C. J. Hogeboom, K. J. Sherman, and D. C. Cherkin, "Variation in diagnosis and treatment of chronic low back pain by traditional Chinese medicine acupuncturists," *Complementary Ther. Medicine* **9**(3), 154–166 (2001).
9. J. Koo and S. Arain, "Traditional Chinese medicine for the treatment of dermatologic disorders," *Arch. Dermatol.* **134**(11), 1388–1393 (1998).
10. J. Koo and S. Arain, "Traditional Chinese medicine in dermatology," *Clin. Dermatol.* **17**(1), 21–27 (1999).
11. R. Lauche, H. Cramer, C. Hohmann, K. E. Choi, T. Rampp, F. J. Saha, F. Musial, J. Langhorst, and G. Dobos, "The effect of traditional cupping on pain and mechanical thresholds in patients with chronic nonspecific neck pain: A randomised controlled pilot study," *Evid. Based Complement. Alternat. Med.* **2012**, 1–10 (2012).
12. A. Michalsen, S. Bock, R. Ludtke, T. Rampp, M. Baecker, J. Bachmann, J. Langhorst, F. Musial, and G. J. Dobos, "Effects of traditional cupping therapy in patients with carpal tunnel syndrome: A randomized controlled trial," *J. Pain* **10**(6), 601–608 (2009).
13. K. J. Sherman, D. C. Cherkin, and C. J. Hogeboom, "The diagnosis and treatment of patients with chronic low-back pain by traditional Chinese medical acupuncturists," *J. Altern. Complement. Med.* **7**(6), 641–650 (2001).
14. J. Wang and X. J. Xiong, "Evidence-based Chinese medicine for hypertension," *Evid. Based Complement. Alternat. Med.* **2013**, 978398 (2013).
15. Y. Wang, X. M. Lin, and G. Q. Zheng, "Traditional Chinese medicine for Parkinson's disease in china and beyond," *J. Altern. Complement. Med.* **17**(5), 385–388 (2011).
16. T. Li, Y. X. Li, Y. Lin, and K. Li, "Significant and sustaining elevation of blood oxygen induced by Chinese cupping therapy as assessed by near-infrared spectroscopy," *Biomed. Opt. Express* **8**(1), 223–229 (2017).
17. C. Y. Gao, M. Wang, L. He, Y. N. He, and T. Li, "Alternations of hemodynamic parameters during Chinese cupping therapy assessed by an embedded near-infrared spectroscopy monitor," *Biomed. Opt. Express* **10**(1), 196–203 (2019).
18. S. Kim, E. Kim, G. Jung, S. Lee, and J. G. Kim, "The hemodynamic changes during cupping therapy monitored by using an optical sensor embedded cup," *J. Biophotonics* **12**(5), e201800286 (2019).
19. L. H. V. Wang and S. Hu, "Photoacoustic tomography: In vivo imaging from organelles to organs," *Science* **335**(6075), 1458–1462 (2012).
20. L. V. Wang, "Multiscale photoacoustic microscopy and computed tomography," *Nat. Photonics* **3**(9), 503–509 (2009).
21. P. Lai, L. Wang, J. W. Tay, and L. V. Wang, "Photoacoustically guided wavefront shaping for enhanced optical focusing in scattering media," *Nat. Photonics* **9**(2), 126–132 (2015).
22. P. K. Upputuri and M. Pramanik, "Recent advances toward preclinical and clinical translation of photoacoustic tomography: a review," *J. Biomed. Opt.* **22**(4), 041006 (2016).

23. H. Li, F. Cao, Y. Zhou, Z. Yu, and P. Lai, "Interferometry-free noncontact photoacoustic detection method based on speckle correlation change," *Opt. Lett.* **44**(22), 5481–5484 (2019).
24. X. Huang, W. Shang, H. Deng, Y. Zhou, F. Cao, C. Fang, P. Lai, and J. Tian, "Clothing spiny nanoprobe against the mononuclear phagocyte system clearance in vivo: Photoacoustic diagnosis and photothermal treatment of early stage liver cancer with erythrocyte membrane-camouflaged gold nanostars," *Appl. Mater. Today* **18**, 100484 (2020).
25. Y. J. Liu, H. H. Liu, H. X. Yan, Y. C. Liu, J. S. Zhang, W. J. Shan, P. X. Lai, H. H. Li, L. Ren, Z. J. Li, and L. M. Nie, "Aggregation-induced absorption enhancement for deep near-infrared photoacoustic imaging of brain gliomas in vivo," *Adv. Sci.* **6**(8), 1801615 (2019).
26. H. F. Zhang, K. Maslov, G. Stoica, and L. H. V. Wang, "Functional photoacoustic microscopy for high-resolution and noninvasive in vivo imaging," *Nat. Biotechnol.* **24**(7), 848–851 (2006).
27. F. Cao, Z. H. Qiu, H. H. Li, and P. X. Lai, "Photoacoustic imaging in oxygen detection," *Appl. Sci.* **7**(12), 1262 (2017).
28. J. F. Andersen, J. Busck, and H. Heiselberg, "Pulsed Raman fiber laser and multispectral imaging in three dimensions," *Appl. Opt.* **45**(24), 6198–6204 (2006).
29. L. de la Cruz-May, J. A. Alvarez-Chavez, E. B. Mejia, A. Flores-Gil, F. Mendez-Martinez, and S. Wabnitz, "Raman threshold for nth-order cascade Raman amplification," *Opt. Fiber Technol.* **17**(3), 214–217 (2011).
30. N. Bosschaert, G. J. Edelman, M. C. G. Aalders, T. G. van Leeuwen, and D. J. Faber, "A literature review and novel theoretical approach on the optical properties of whole blood," *Lasers Med. Sci.* **29**(2), 453–479 (2014).
31. Y. Z. Liang, L. Jin, B. O. Guan, and L. D. Wang, "2 MHz multi-wavelength pulsed laser for functional photoacoustic microscopy," *Opt. Lett.* **42**(7), 1452–1455 (2017).